

Dalton Transactions

Accepted Manuscript



This is an *Accepted Manuscript*, which has been through the Royal Society of Chemistry peer review process and has been accepted for publication.

Accepted Manuscripts are published online shortly after acceptance, before technical editing, formatting and proof reading. Using this free service, authors can make their results available to the community, in citable form, before we publish the edited article. We will replace this *Accepted Manuscript* with the edited and formatted *Advance Article* as soon as it is available.

You can find more information about *Accepted Manuscripts* in the [Information for Authors](#).

Please note that technical editing may introduce minor changes to the text and/or graphics, which may alter content. The journal's standard [Terms & Conditions](#) and the [Ethical guidelines](#) still apply. In no event shall the Royal Society of Chemistry be held responsible for any errors or omissions in this *Accepted Manuscript* or any consequences arising from the use of any information it contains.

Ultrafast Electronic and Vibrational Relaxations in Mixed-Ligand Dithione-Dithiolato Ni, Pd, and Pt Complexes

Franziska Frei,¹ Ariana Rondi,¹ Davide Espa,² Maria Laura Mercuri,² Luca Pilia,³
Angela Serpe,² Ahmad Odeh,⁴ Frank Van Mourik,⁴ Majed Chergui,⁴ Thomas Feurer,¹
Paola Deplano,^{*,2} Antonín Vlček, Jr.,^{*,5,6} Andrea Cannizzo^{*,1}

¹ Institute of Applied Physics, University of Bern, Sidlerstrasse 5, CH-3012 Bern, Switzerland

² Dipartimento di Scienze Chimiche e Geologiche, Research Unit of INSTM, Università di Cagliari, I-09042 Monserrato, Cagliari, Italy

³ Dipartimento di Ingegneria Meccanica Chimica e dei Materiali, Università di Cagliari, via Marengo 2, I09123, Cagliari, Italy

⁴ Ecole Polytechnique Fédérale de Lausanne (EPFL), Laboratoire de Spectroscopie Ultrarapide (LSU), ISIC, Faculté des Sciences de Base, Station 6, CH-1015 Lausanne-Dorigny, Switzerland

⁵ J. Heyrovský Institute of Physical Chemistry, Academy of Sciences of the Czech Republic, Dolejškova 3, 182 23 Prague, Czech Republic

⁶ Queen Mary University of London, School of Biological and Chemical Sciences, Mile End Road, London, E1 4NS, UK

e-mail: andrea.cannizzo@iap.unibe.ch, deplano@unica.it, a.vlcek@qmul.ac.uk

Abstract

Ultrafast excited-state dynamics of planar Pt, Pd, and Ni dithione-dithiolato complexes were investigated using transient absorption spectroscopy on the femtosecond - picosecond timescale. All studied complexes show a common photobehaviour, although individual kinetics parameters and quantum yields vary with the metal, the dithione ligand and, namely, the solvent (DMF, MeCN). Laser pulse irradiation at 800 nm populates the lowest singlet excited state of a dithiolato→dithione charge transfer character, ¹LL'CT. The optically excited state undergoes a solvation-driven sub-picosecond electronic relaxation that enhances the dithione/dithiolato charge separation. The ¹LL'CT state decays with a 1.9 - 4.5 ps lifetime by two simultaneous pathways: intersystem crossing (ISC) to the lowest triplet state ³LL'CT, and nonradiative decay to the ground state. ISC occurs on a ~6 ps timescale, virtually independent of the metal, whereas the rate of the nonradiative decay to the ground state decreases on going from Ni (2 ps) to Pd (3 ps) and Pt (~10 ps). ³LL'CT is initially formed

vibrationally excited. Its equilibration (cooling) takes place on a picosecond timescale and is accompanied by a competitive decay to the ground state. Equilibrated $^3\text{LL}'\text{CT}$ is populated with a quantum yield of less than 50%, depending on the metal: $\text{Pt} > \text{Pd} > \text{Ni}$. $^3\text{LL}'\text{CT}$ is long-lived for Pt and Pd ($\gg 500$ ps) and short lived for Ni (~ 15 ps). Some of the investigated complexes also exhibit spectral changes due to vibrational cooling of the singlet (2-3 ps, depending on the solvent). Rotational diffusion occurs with lifetimes in the 120-200 ps range. Changing the dithione ($\text{Bz}_2\text{pipdt}/^i\text{Pr}_2\text{pipdt}$) as well as dithiolate/diselenolate (dmit/dsit) ligands has only small effects on the photobehavior. It is proposed that the investigated dithione-dithiolato complexes could act as photooxidants ($*E^0 \approx +1.2$ V vs. NHE) utilizing their lowest excited singlet ($^1\text{LL}'\text{CT}$), provided that the excited-state state electron transfer is ultrafast, competitive with the picosecond decay. On the other hand, efficiency of any triplet-based processes would be severely limited by the low quantum yield of triplet population.

Introduction

Since decades, metal complexes have been at the centre of intense research activity aimed at understanding their rich photophysics and developing their great potential for applications in molecular photonics, electronics, and solar energy harnessing.¹ In the description of their physicochemical processes, it is conventionally supposed that ground- and excited-state processes are localized either at the metal atom or at the ligands. This is equivalent to assuming that the oxidation state of the central metal atom and the ligands are well defined. Although this is the most common case, in several classes of coordination complexes the oxidation states are impossible to be determined unambiguously, usually because of a strong metal-ligand electronic delocalization and/or the metal and ligand orbitals occurring in the same energy range. In these cases, ligands are commonly called "*non-innocent*". This term should more correctly refer to a particular combination of the ligand and

the metal rather than to the ligand alone, since the same ligand can behave as innocent or non-innocent depending on the metal involved.²⁻⁶ In these compounds, redox changes as well as electronic excitations could be delocalized over the whole metal-ligand moiety. In fact, an increasing number of coordination compounds are now being recognized to show a non-innocent behaviour, whose consequences and applications have been summarized in a special issue of *Coordination Chemistry Reviews* (2010, Vol. 254, Issue 13-14).

Metal dithiolene complexes are a paradigmatic case of "noninnocent" species and their bonding, metal and ligand oxidation states, electron density distribution, as well as assignments of strong UV-vis-NIR absorption and multiple electrochemical redox steps are being debated since their discovery in the early 60's.^{2, 3, 7, 8}

A very interesting case is presented by d⁸ metal complexes which combine in their coordination spheres an electron-rich dianionic dithiolato (or diselenolato) ligand dmit/dsit²⁻ with an electron accepting dithione ligand R₂pipdt, formally [M(II)(R₂pipdt)(dmit/dsit²⁻)] (M = Pt, Pd, Ni; Figure 1).⁹⁻¹⁶ These complexes may be viewed as ligand-based intervalence compounds where the two dithiolene ligands occur in formally different oxidation states: a reducing dianionic dithiolate/diselenolate making a prevailing contribution to the HOMO; and an oxidizing neutral dithione making a prevailing contribution to the LUMO (Figure S1).^{12, 14, 15} Metal contributions are relatively small: <20% in HOMO and <10% in LUMO, depending on the particular complex.^{12, 14, 15} These complexes show an intense solvatochromic NIR absorption band in the 750-900 nm range that originates from the HOMO→LUMO transition of a predominantly dithiolato→dithione ligand to ligand charge transfer (LL'CT) character (or, given a small change in metal participation, a mixed metal-ligand to ligand charge transfer term is also used, abbreviated MMLL'CT).^{9, 11, 12, 14} Such a transition results in a large electron density redistribution in the complex molecule and a large change of the molecular dipole moment, up to 11 D,⁹ and giving rise to prominent second-order nonlinear optical

properties, namely an exceptionally high quadratic hyperpolarizability.^{9, 12, 14, 15} Electrochemical reduction of these complexes is localized predominantly at the dithione ligand and shifts the intense visible band to higher energies and reversibly switches the nonlinear optical activity.^{11, 13} The strong negative solvatochromism of dithione-dithiolato complexes^{9, 12} is another interesting feature that reflects the large change in solvation upon electronic excitation, due to changing the molecular polarity. Interestingly, solvent-dependent DFT and TDDFT calculations have revealed that the interaction with the solvent increases the HOMO and LUMO localization at the dithiolato and dithione ligand, respectively.¹²⁻¹⁴ One can thus argue that solvation and its changes upon excitation are important factors determining electronic (de)localization and, hence, the "non-innocence" of the metal-dithiolene moieties.

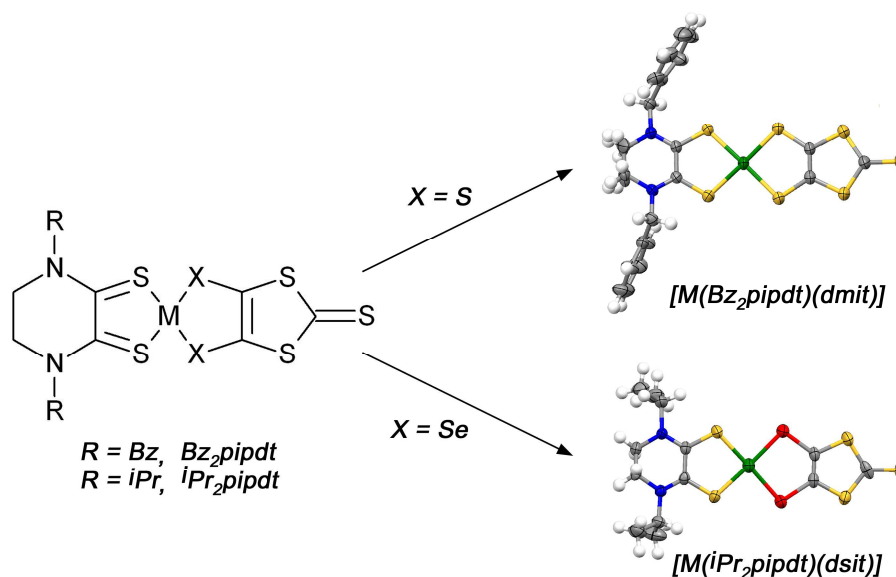


Figure 1. Structures of the investigated complexes $[M(Bz_2pipdt)(dmit)]$ and $[M(iPr_2pipdt)(dmit)]$. $M(II) = Ni, Pd, Pt$. Left: a generic structure; Right: molecular structures of $[Pt(Bz_2pipdt)(dmit)]$ and $[Pt(Bz_2pipdt)(dsit)]$.

Strong absorption in the UV-vis-NIR range, solvatochromism, redox activity, and tuneable photonic properties make metal dithiolene complexes prime candidates for photophysical investigations. Characterizing their electronic excited states as well as

relaxation and deactivation pathways could enable new applications as photocatalysts and sensitizers of light-energy harvesting processes (indicated¹⁷⁻¹⁹ for similar Pt diimine-dithiolates). Investigating time-dependent solvation triggered by laser pulse excitation will contribute to our understanding of the dynamics of solvent-solute interactions and solvation-induced changes in the solute electronic structure. Despite these challenges, the photocycle of metal dithiolenes is virtually unknown. Most of these complexes are non-emissive, indicating short-lived excited states decaying by fast nonradiative pathways. Still, the lack of emission and short excited-state lifetimes do not preclude interesting photoreactivity and rich excited-state dynamics.

Herein, we have investigated the photocycle of a series of group 10 metal dithione-dithiolato complexes, triggered by 800 nm femtosecond laser pulse excitation into the the lowest absorption band. The resulting excited-state dynamics were investigated using time-resolved absorption spectroscopy (TA), whereby difference visible absorption spectra were measured at selected times after excitation and the spectral time evolution was analyzed by global fitting and singular value decomposition methods. In particular, we report on the excited-state dynamics of mixed-ligand Ni, Pd, and Pt complexes combining electron-accepting dithiones Bz₂pipdt (1,4-dibenzylpiperazine-2,3-dithione) or ⁱPr₂pipdt (1,4-diisopropylpiperazine-2,3-dithione) with an electron-donating dithiolate dmit (2-thioxo-1,3-dithiole-4,5-dithiolato) or diselenolate dsit (2-thioxo-1,3-dithiole-4,5-diselenolato) (Figure 1). In this research, we aim at understanding the nature and dynamics of non-radiative deactivation channels and the role of the electron withdrawing or donating character of the dithiolene ligands, the central metal atom, as well as of the solvent.

Experimental

Materials. The investigated complexes were synthesized and characterized by published procedures.^{11, 13} The solvents acetonitrile (MeCN) and *N,N*-dimethylformamide (DMF) were of spectroscopic quality (Aldrich).

Instrumentation. The setup for transient absorption (TA) studies was described before.^{20, 21} The sample solutions were excited (pumped) at 800 nm with 100 fs pulses focused to a ~ 200 μm diameter spot. Energy per pulse was typically 1 μJ . The probe consisted of a white-light continuum generated by focusing a small part of the 800 nm Ti:Sapphire laser output onto a 1 mm thick CaF_2 window. The probe spot at the sample position was ~ 70 μm in diameter. The probe beam was dispersed after the sample in a 0.3 m monochromator and detected by a 512 pixel photodiode array model Hamamatsu S11105 covering a spectral range from 400 to 800 nm. The cross-correlation time of the experimental setup was ~ 130 fs, but a non-negligible cross-phase modulation affected measurements from -200 to 200 fs. A mechanical chopper placed along the pump beam path and synchronized at half the repetition rate of the laser was used for alternating between "pumped" and "unpumped" measurements of the transmission of the probe light through the sample. The polarizations of the pump and probe beams was set parallel. The group velocity dispersion (GVD) of the probe pulse was measured separately in pure solvents and used to correct the TA spectra for the time zero displacement at different wavelengths. Special care was taken to work in a linear regime, where the TA signal is proportional to the pump and probe beam energies. For few samples, we verified that the detected signals were linear with the solute concentration. To avoid photodegradation, sample solutions were flowed with a peristaltic pump through an UV-grade flow cell with an internal path of 500 μm . The concentration was adjusted to ~ 0.3 OD at 800 nm. Visible absorption spectra measured before and after TA measurements showed no changes, indicating a remarkable photostability of the investigated complexes.

Steady-state optical absorption spectra were measured on a Shimadzu UV-3600 spectrometer. Scans covered the 250-1000 nm range with a 1 nm step.

Data analysis. All data were corrected for GVD. To avoid possible artefacts due to cross-phase modulation, data points from -200 to 200 fs were neglected during the kinetics fitting. Data were analyzed in two different ways that are expected to converge to the same result: i) kinetic traces at relevant wavelengths (maxima, minima, half maxima and minima, and close to the zero signal axis) were extracted from the data and then simultaneously fitted with a suitable number of exponential decays. During the optimization procedure, the instrumental response function (irf) and time constants were considered as global parameters (i.e., the same for all the wavelengths), while amplitudes were treated as local parameters. A sum of 5 exponentials was found enough to fit all the traces; ii) a Singular Value Decomposition (SVD) analysis was carried out to decompose all the time-wavelength data ($\Delta Abs(\lambda, t)$, after irf deconvolution) into a minimal number of spectra (so-called Decay Associated Spectra or DAS), each undergoing an exponential decay with its own lifetime:²²

$$\Delta Abs(\lambda, t) = \sum DAS_i(\lambda) \cdot \exp(-t/\tau_i) \quad (1)$$

Since both methods provided consistent pictures, hereinafter we will show only the outcomes of SVD analyses.

Results and Discussion

Ground-state visible absorption spectra of all the samples show two bands around 800 and 480 nm with comparable molar absorptivities and minor variations from sample to sample (Figure 2). Accordingly to DFT calculations,^{9, 12, 14, 15} the ~800 nm band corresponds to the HOMO→LUMO transition (Figure S1) into the lowest singlet excited state (S_1) of a ¹LL'CT character. The electron density is transferred from the dithiolato/diselenolato ligand (dmit/dsit) to the electron withdrawing dithione (Bz₂pipdt/ ¹Pr₂pipdt), plus a small

M→dithione MLCT contribution. The second absorption band is assigned to a highly mixed transition of a LL'CT/IL(R₂pipdt) character, as was calculated for [Pt(Bz₂pipdt)(dmit)].¹⁵ Changing the solvent from DMF to MeCN has only a very small effect on the absorption spectra, as is demonstrated for [Pt(ⁱPr₂pipdt)(dmit)] in Figure S2, in accordance with comparable polarity of these two solvents.

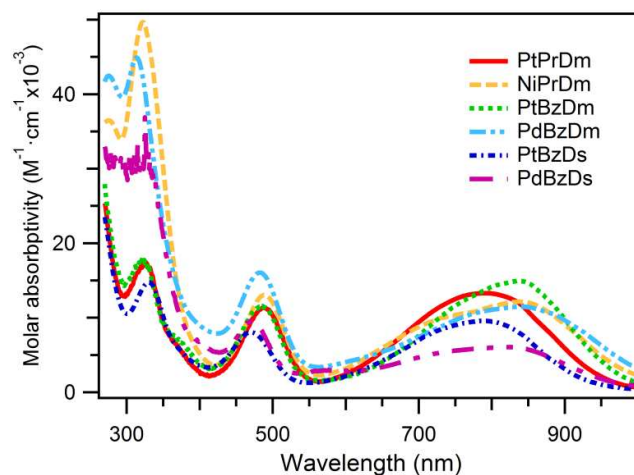


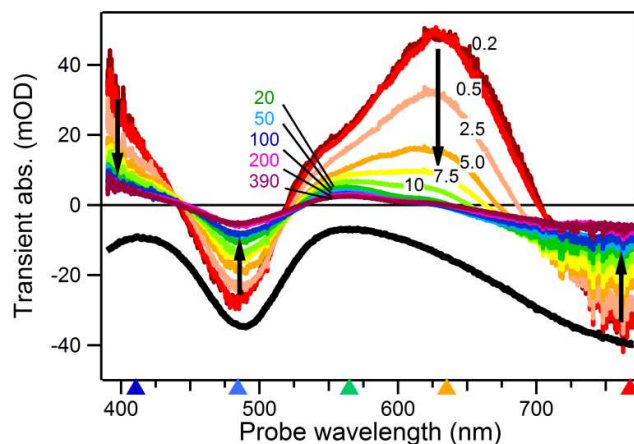
Figure 2. Steady-state absorption spectra of the investigated samples in DMF. Pr = ⁱPr₂pipdt; Bz = Bz₂pipdt; Dm = dmit; Ds = Dsit. (For a [Pt(ⁱPr₂pipdt)(dmit)] spectrum in MeCN see Figure S2.)

In terms of photoinduced behaviour, all the samples show common patterns of TA spectra and decay kinetics. Thus, we will first discuss in detail [Pt(ⁱPr₂pipdt)(dmit)] that represents the behaviour of all the other samples. Then, we will outline the structural effects of changing the Pr/Bz substituent on the pipdt dithione ligand, replacing the dithiolate (dmit) by a diselenolate (dsit), and changing the metal atom from Ni to Pd and Pt.

Photocycle and relaxation mechanism of [Pt(ⁱPr₂pipdt)(dmit)]

Figure 3 shows a selection of TA spectra of [Pt(ⁱPr₂pipdt)(dmit)] in DMF at different pump-probe time delays and kinetic traces measured at selected probe wavelengths. The spectral evolution is also visualized in the form of a wavelength-time 2D plot in Figure S3. A

strong excited-state absorption (ESA) develops within the instrument time resolution, characterized by a broad band around 630 nm and absorption below 440 nm that increases into the UV region. After the initial period of the first few hundreds of femtoseconds where the signal stays nearly constant, most of the ESA decays in less than 10 ps, leaving a weak long-lasting ($\gg 500$ ps) component whose spectrum is different from the initial transient. The negative bands at 480 nm and ≥ 700 nm closely match the inverted steady-state absorption spectrum and are therefore attributed to the bleached ground-state absorption (GSB). Kinetic traces due to positive and negative signals differ during the first 10 ps but follow the same temporal evolution at later times. Using the SVD data analysis, the TA data were spectrally decomposed into five DASs (Figure 4), each decaying with its own lifetime: 760 fs, 3.42 ps, 9.4 ps, 188 ps, and ∞ .



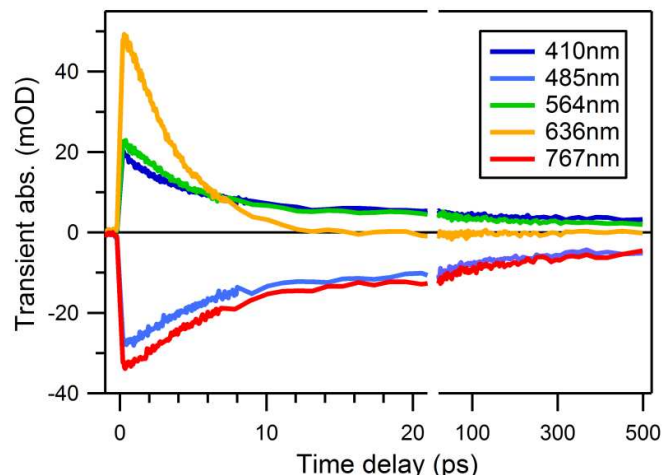


Figure 3. Representative selection of transient absorption (TA) spectra at different time delays (top) and kinetic traces (bottom) of $[\text{Pt}(\text{}^1\text{Pr}_2\text{pipdt})(\text{dmit})]$ in DMF, obtained upon 800 nm excitation. The black curve in the top panel shows an inverted ground-state absorption spectrum. The black arrows indicate the evolution of the different bands with time. Triangles on the horizontal axis denote the wavelengths of the kinetic traces shown in the bottom panel. (See Figure S2 for a complete wavelength time 2D plot.)

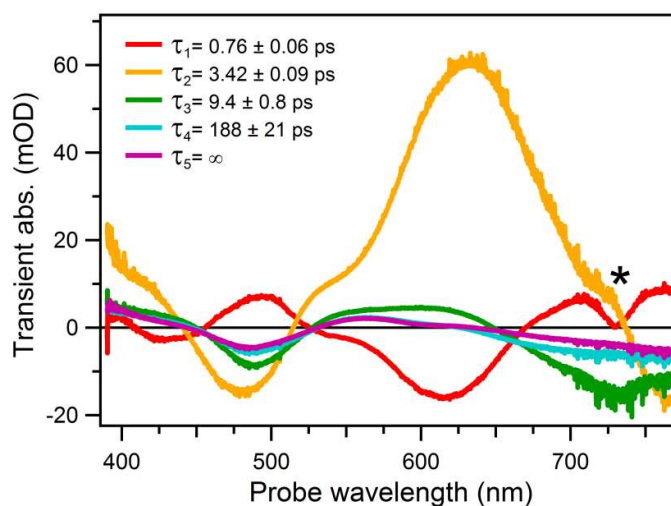


Figure 4. Decay associated spectra (DAS) obtained by SVD analysis of TA spectra of $[\text{Pt}(\text{}^1\text{Pr}_2\text{pipdt})(\text{dmit})]$ in DMF (Figure 3 and S3). Each curve is labelled with the respective time constant. τ_5 describes a contribution with dynamics much longer than the scanned interval and is modelled with a step function. *An SVD-analysis artefact. (See Figure S4 for successive DASs sums indicating spectral changes due to individual kinetics steps.)

The 760 fs DAS shows nearly the same shape as the 3.4 ps DAS but with an inverted sign (Figure 4), indicating a signal rise occurring with a 700-800 fs lifetime. As will be shown

later, it is attributable to solvation-induced charge redistribution in the optically populated S_1 state. Combination of the 760 fs rise and 3.4 ps decay kinetics explains the lack of spectral evolution apparent in the sub-picosecond range (Figure 3). The 3.4 ps DAS describes the decay of the main transient band at ~ 640 nm and of the blue-most band, accompanied by a partial recovery of the negative bleach signals. The 3.4 ps decay lifetime is much faster than the ~ 5 ns radiative fluorescence lifetime (estimated from the ground-state absorption band area), allowing us to estimate the fluorescence quantum yield of about 5×10^{-4} , in agreement with the lack of any appreciable steady-state fluorescence. The 3.4 ps component corresponds to the population decay of the S_1 state. We also observe a $\sim 40\%$ recovery of the bleach signal with the same time constant (see kinetic traces at 410 nm and 767 nm in Figures 3 and S4), revealing that S_1 decays by two parallel nonradiative pathways to the ground state and to a lower-lying excited state with a comparable branching ratio. The temporal evolution of the lower state is described by the remaining three DASs (τ_3 , τ_4 , τ_5). The corresponding spectral patterns are weaker than the initial one (τ_1 , τ_2) and the main ESA band is blue-shifted to about 570 nm. Both patterns show a positive absorption below 450 nm. Since the 800 nm excitation populates the lowest singlet excited state, we attribute the later-time ESA features to the corresponding triplet T_1 of a $^3LL'$ CT character. This assignment is corroborated by the qualitative similarity with the S_1 spectral pattern. Spectra of both excited states show absorption between 500 and 650 nm that is typical for a reduced dithione ligand¹¹ present in the singlet as well as triplet LL' CT states (both formally viewed as $^*[Pt(iPr_2pipdt^{\bullet-})(dmit^{\bullet-})]$). Observation of a slow direct decay to the ground state ($\tau_5 \gg 500$ ps) confirms that the second excited state is the lowest excited state of the molecule, again in line with its T_1 assignment (i.e., $^3LL'$ CT).

The τ_3 component of 9.4 ps manifests narrowing and blue-shifting of the T_1 ESA band (Figures 4, S4), indicative of a vibrational relaxation by energy transfer to the solvent. This

assignment is supported by measurements in MeCN, discussed below. It is accompanied by a partial decrease of the bleach (Figure 4 and Figures S4), suggesting a competitive ground-state recovery from hot T_1 levels. The 188 ps lifetime is typical of rotational diffusion and, accordingly, it is not accompanied by any change of the spectral pattern. (A pure rotational diffusion should decrease the signal by a factor of 3 rather than the observed ~ 2 (Figure S4). We tentatively assign this mismatch to a not perfect disentanglement of the two longest decay components.) The τ_5 (∞) DAS corresponds to the difference absorption spectrum of a fully equilibrated T_1 state. The long-time ESA decay mirrors the kinetics of the bleach recovery, demonstrating that the triplet state decays directly to the ground state. (Compare the positive decays at 410 and 564 nm with the negative traces at 485 and 767 nm in Figure 3, due to ESA and GSB, respectively.)

The temporal evolution of the TA spectra described above shows several fast steps involving changes in the bleach signal intensity, which we attribute to relaxation processes (τ_1 rise) and to a nonradiative decay of S_1 and hot T_1 states to the ground state (τ_2 and τ_3 decays, respectively). Since we are probing at wavelengths shorter than the pump (800 nm), we can safely rule out any contributions due to stimulated emission to the bleach kinetics.

In order to clarify which steps are related to solvation dynamics, we compared the behaviour of $[\text{Pt}(\text{Pr}_2\text{pipdt})(\text{dmit})]$ in DMF (Figures 3, 4, S3, S4) and MeCN (Figures 5, S5). These two solvents have comparable permanent dipole moments and static dielectric constants while MeCN shows faster solvation response (150 fs) than DMF (670 fs).²³ Static (Figure S2) as well as transient absorption spectra show very similar spectral patterns in the two solvents, indicating the same characters of electronic transitions and excited states. However, the SVD analysis reveals important kinetics differences, in particular for the picosecond components. The 300 fs DAS in MeCN is spectrally similar to the 760 fs DAS in DMF (compare also the spectra at 200 fs and at 500 fs in Figures 3 and 5), whereas the

1.75 and 3.37 ps DASs in MeCN seem to describe a significantly different dynamical behaviour than the 3.42 and 9.4 ps DASs in DMF. In the case of MeCN, the 1.75 ps τ_2 component describes an ESA blue-shift and narrowing that is typical of a cooling process, followed by a population decay of 3.37 ps. (This is clearly demonstrated by the DAS sums shown in Figure S5.) No spectral evolution similar to the 9.4 ps DMF component was observed in MeCN. Moving to longer components, they describe a biphasic recovery of 2/3 of the GSB signal due to rotational diffusion (τ_4 , τ_5), and the slow ($>>500$ ps) decay of the triplet state (τ_6).

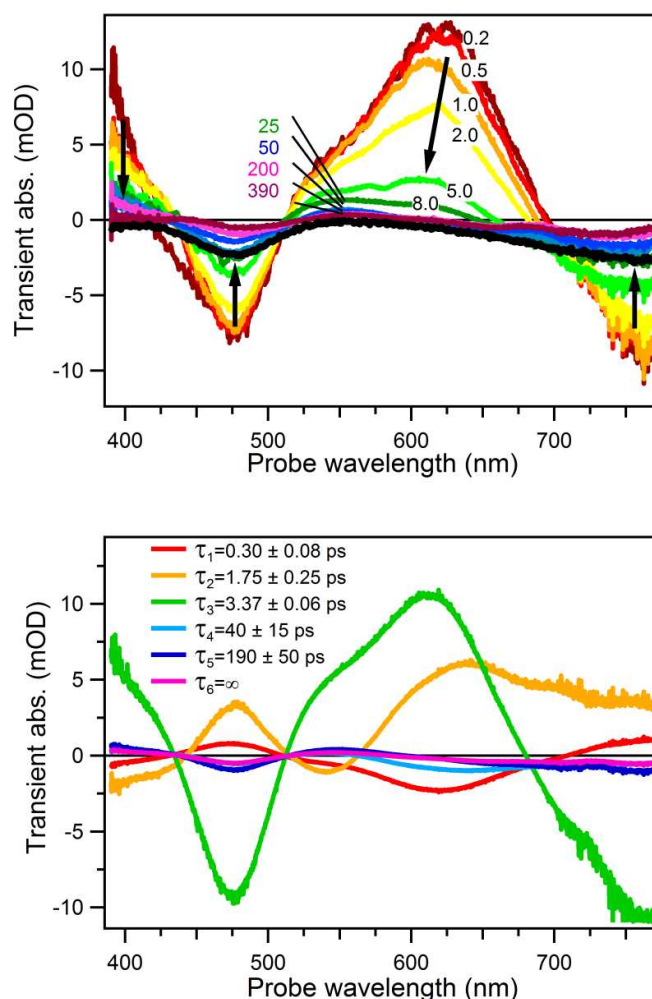


Figure 5. Top: Representative selection of transient absorption (TA) spectra at different time delays (top) and kinetics traces (bottom) of $[\text{Pt}(\text{}^1\text{Pr}_2\text{pipdt})(\text{dmit})]$ in MeCN, obtained upon 800 nm excitation. The black curve in the top panel shows the inverted ground-state absorption spectrum. The black arrows indicate the evolution of different bands with time.

Bottom: DAS spectra obtained by SVD analysis. (See Figure S5 for successive DASs sums indicating spectral changes due to individual kinetics steps.)

To elucidate the difference between the picosecond components in the two solvents, we compare in Figure 6 the 3.42 ps DAS in DMF with the sum of the 1.75 and 3.37 ps DASs in MeCN, which represent the overall spectral changes due to these two kinetics components. The match between them is excellent and reveals that the 3.42 ps DAS in DMF is not a pure ESA decay but actually describes a complex behaviour whereby a population decay and solvent relaxation occur accidentally with comparable rates. The relaxation rate scales with the solvation response time, whereas the S_1 decay lifetime is ~ 3.4 ps, regardless of the solvent. Hence, the two processes become kinetically separated in MeCN where the solvent relaxation is much faster. A similar dependence on the solvent response time is observed in the femtosecond time range (τ_1), where the rise of the ESA signal and GSB deepening is twice faster in MeCN than in DMF. The τ_1 values (760 and 300 fs in DMF and MeCN, respectively) scale with the solvation times (670 fs and 150 fs, resp.²³), indicating a solvation-driven process. The ESA rise suggests that the excited-state electronic wave function changes in the course of the solvent relaxation that appears to drive the localization of the excited electron density on the dithione ligand.

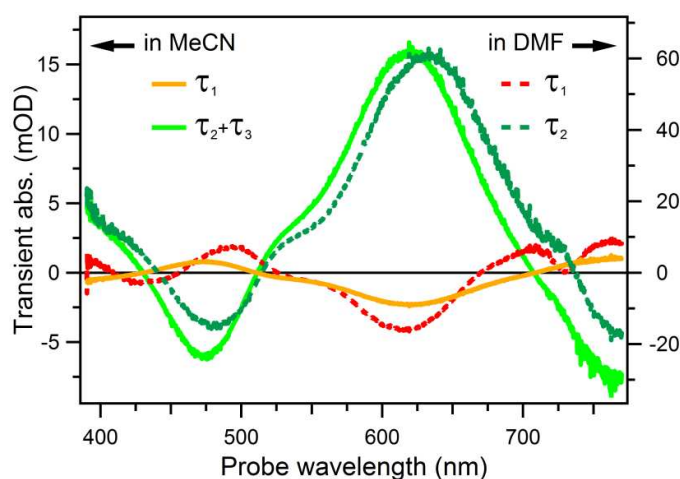


Figure 6. Comparison of the femtosecond (τ_1) and picosecond (τ_2 and τ_3) DASs of [Pt(¹Pr₂pipdt)(dmit)] in DMF (dashed lines, right axis) and MeCN (solid lines, left axis), taken from Figures 4 and 5, respectively. For comparisons purposes, the sum of the two picosecond components in acetonitrile is shown, and the first DAS in acetonitrile is multiplied by a factor of 2.

The temporal spectral evolution in MeCN does not contain any component similar to the 9.4 ps τ_3 DAS that was observed in DMF and attributed to the T₁ vibrational relaxation (cooling). This observation rules out an alternative hypothesis that the 9.4 ps τ_3 process in DMF involves an intermediate electronic excited state (that would occur in both solvents). It appears that the T₁ cooling in MeCN is faster than in DMF, its rate being comparable to or faster than that of the singlet-state decay, i.e. ~3.4 ps.

This experimental behaviour suggests a rather simple photocycle, depicted in Figure 7: irradiation of the ground state (GS) into the lowest allowed transition produces the lowest singlet excited state S₁ identified as dmit/dsit→R₂pipdt ¹LL'CT. The extent of the charge separation increases in the course of solvent dielectric reorganization (τ_{solv}). Vibrational relaxation (cooling, τ_{SVR}) of the singlet excited state occurs on a 1–3 ps timescale by vibrational energy transfer to the solvent. The S₁ population decays with a lifetime τ_{S} (~3.4 ps) into hot levels of the lowest triplet state ([#]T₁), by a ~55% efficient inter-system crossing (τ_{ISC}) and simultaneously into the ground state (τ_{nr}). [#]T₁ undergoes cooling (τ_{TVR}) producing an equilibrated T₁ state that is established in less than 10 ps (depending on the solvent). The [#]T₁ cooling is accompanied by a partial ground-state recovery, diminishing the final T₁ yield to about 30%. Nonradiative decay of hot [#]T₁ levels is much faster (≤ 10 ps) than of equilibrated T₁ ($\gg 500$ ps). This mechanism is qualitatively valid for all the investigated complexes, although with quantitative differences in the kinetics and quantum yields. The experimental values obtained are summarized in Table 1.

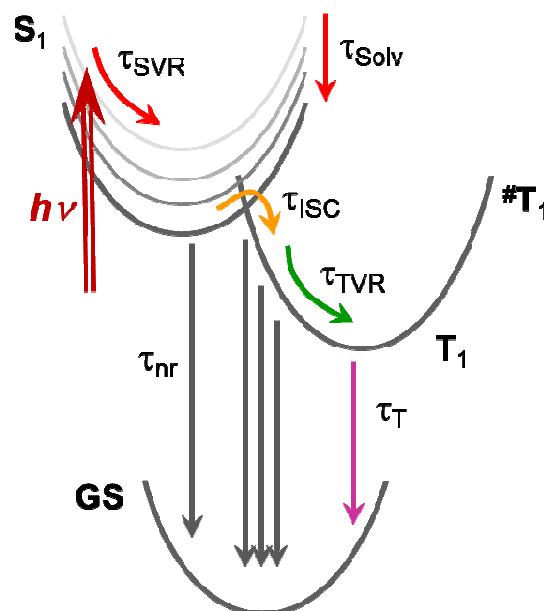


Figure 7. Photocycle of the complexes $[M(R_2\text{pipdt})(\text{dmit}/\text{dsit})]$ upon 800 nm excitation into the lowest $^1\text{LL}^{\prime}\text{CT}$ excited state (dark red arrow). The colours of arrows representing individual relaxation steps match the colours of the corresponding DASs in Figures 4 and 5.

Table 1. Summary of kinetics parameters determined by SVD analysis of TA spectra measured in DMF, unless stated otherwise. The different time constants are named accordingly to Figure 7.

Sample	τ_{Sol}	τ_{SVR}	τ_{S}	τ_{IVR}	τ_{Rot}	$\text{QY}_{\text{S}\rightarrow\#\text{T}}$	$\text{QY}_{\#\text{T}\rightarrow\text{T}}$	$\text{QY}_{\text{S}\rightarrow\text{T}}$
$[\text{Pt}(\text{Pr}_2\text{pipdt})(\text{dmit})]$	0.76 ± 0.06	~ 3.4	3.42 ± 0.09	9.4 ± 0.8	188 ± 21	55%	50%	30%
$[\text{Pt}(\text{Pr}_2\text{pipdt})(\text{dmit})]$ in MeCN	0.30 ± 0.08	1.75 ± 0.25	3.37 ± 0.06	a	40 ± 15 190 ± 50	-	-	20%
$[\text{Ni}(\text{Pr}_2\text{pipdt})(\text{dmit})]$	0.37 ± 0.03	-	1.44 ± 0.05	14.8 ± 0.3	-	25%	0%	0%
$[\text{Pt}(\text{Bz}_2\text{pipdt})(\text{dmit})]$	0.75 ± 0.03	2.75 ± 0.03	4.53 ± 0.02	a	125 ± 4	-	-	25%
$[\text{Pt}(\text{Bz}_2\text{pipdt})(\text{dsit})]$	0.57 ± 0.06	-	4.3 ± 0.1	7.1 ± 0.5	182 ± 6	75%	60%	50%
$[\text{Pd}(\text{Bz}_2\text{pipdt})(\text{dmit})]$	0.61 ± 0.03	-	1.89 ± 0.03	15.2 ± 0.4	42 ± 8	33%	25%	8%
$[\text{Pd}(\text{Bz}_2\text{pipdt})(\text{dsit})]$	0.80 ± 0.04	-	1.96 ± 0.05	18.3 ± 0.3	142 ± 9	33%	25%	8%

a: Not observed, presumably comparable with τ_{S} .

Structural effects on the photodynamics: the dithione ligand.

Replacing the $^i\text{Pr}_2\text{pipdt}$ dithione ligand with the more electron-withdrawing Bz_2pipdt is expected to increase the localization of the excited electron density on the dithione part of the molecule, enhancing the charge separation upon excitation. The behaviour of

[Pt(Bz₂pipdt)(dmit)] in DMF (Figures 8-left and S6) is similar to that of [Pt(¹Pr₂pipdt)(dmit)]. Namely, the femtosecond solvation-induced signal rise of [Pt(Bz₂pipdt)(dmit)] occurs with a nearly identical time constant of 750 fs. The S₁ lifetime is somewhat longer, (τ_3 , 4.5 ps). The 2.8 ps kinetics component τ_2 , manifested by the S₁ ESA blue-shift and narrowing, is very similar to the 1.8 ps component observed for [Pt(¹Pr₂pipdt)(dmit)] in MeCN. No component attributable to triplet-state relaxation has been observed. It follows that increasing the electron withdrawing character of the dithione ligand extends the singlet excited-state lifetime, presumably by slowing the nonradiative decay to the ground state. Vibrational relaxation of both the S₁ and T₁ states appears to be faster in the Bz₂pipdt case, presumably due to stronger solvent-solute interactions involving the benzyl rings and larger charge separation in the excited-state.

Structural effects on the photodynamics: dithiolato vs. diselenolato ligand.

Replacing the sulfur-coordinated dmit ligands by selenium-coordinated dsit affects more the excited-state spectrum than the kinetics. Namely, the main S₁ ESA band of [Pt(Bz₂pipdt)(dsit)] is broader than in the case of [Pt(Bz₂pipdt)(dmit)] and the intensity is redistributed from the main maximum at about ~630 nm toward the side-band that shifts from 536 to 523 nm (Figures 8, S7). The near-UV ESA band at $\lambda < 450$ nm almost doubles in intensity upon replacing dmit with dsit. These effects are visualized and quantified in Figure S7 by Gaussian decomposition of the TA spectra. SVD analysis (Figure 8 bottom-right) reveals that the [Pt(Bz₂pipdt)(dsit)] photodynamics are very similar to those of [Pt(¹Pr₂pipdt)(dmit)] and [Pt(Bz₂pipdt)(dmit)]: the femtosecond relaxation component is present but slightly faster (570 fs). The S₁ decay is comparable to [Pt(Bz₂pipdt)(dmit)], 4.3 ps. On the other hand, the picosecond relaxation resembles that of [Pt(¹Pr₂pipdt)(dmit)] in DMF:

no component attributable to the S_1 relaxation was found while the 7.1 ps component indicates a T_1 relaxation, comparable to the 9.4 ps process of $[\text{Pt}(\text{}^i\text{Pr}_2\text{pipdt})(\text{dmit})]$.

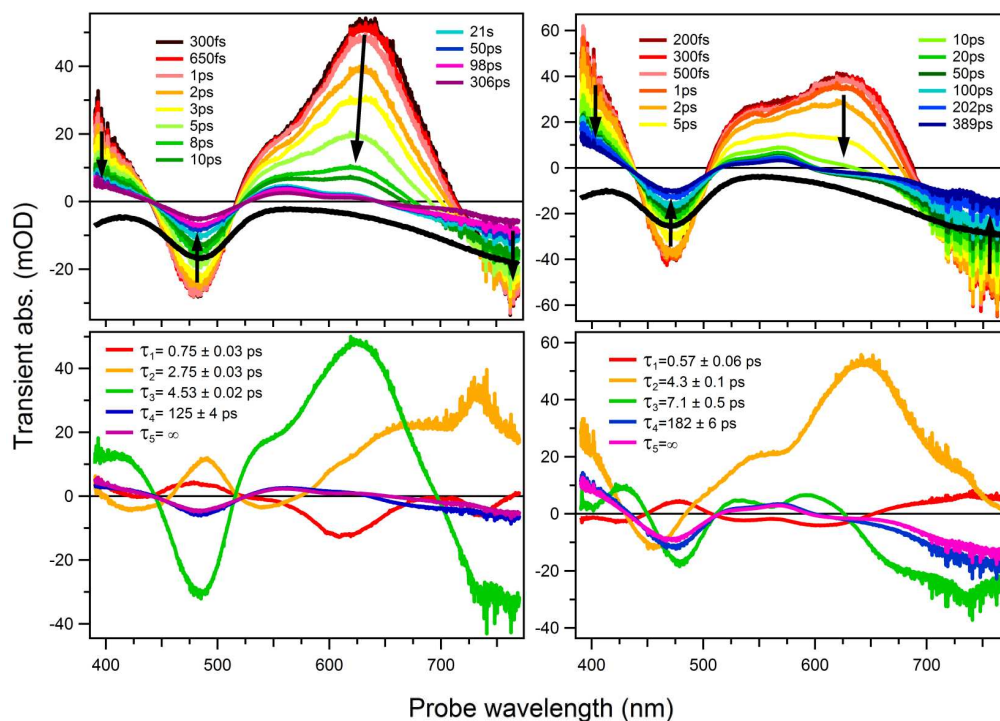


Figure 8. Top: Representative selection of transient absorption (TA) spectra at different time delays (top) of $[\text{Pt}(\text{Bz}_2\text{pipdt})(\text{dmit})]$ (left) and $[\text{Pt}(\text{Bz}_2\text{pipdt})(\text{dsit})]$ (right) in DMF, obtained upon 800 nm excitation. The black curve in the top panels shows an inverted ground-state absorption spectrum. The black arrows indicate the evolution of the different bands with time. Bottom: Decay associated spectra (DAS) labelled according to the respective time constants, obtained by SVD analysis. τ_5 corresponds to the long-lived ($\gg 500$ ps) component, modelled with a step function.

Structural effects on the photodynamics: changing the metal atom Ni, Pd, Pt

To clarify the role of the central metal atom in defining the photophysical properties, we compared the results on the following pairs of complexes: $[\text{Pt}(\text{Bz}_2\text{pipdt})(\text{dmit})]$ / $[\text{Pd}(\text{Bz}_2\text{pipdt})(\text{dmit})]$; $[\text{Pt}(\text{}^i\text{Pr}_2\text{pipdt})(\text{dmit})]$ / $[\text{Ni}(\text{}^i\text{Pr}_2\text{pipdt})(\text{dmit})]$; and $[\text{Pt}(\text{Bz}_2\text{pipdt})(\text{dsit})]$ / $[\text{Pd}(\text{Bz}_2\text{pipdt})(\text{dsit})]$, all in DMF. Experimental spectra and DASs of the Ni and Pd complexes are reported in Figure S8. The TA spectra of all the complexes are qualitatively similar, showing some differences in the relative amplitudes of the near-UV and visible S_1 features at

early time delays. The most pronounced difference is shown by $[\text{Ni}(\text{Pr}_2\text{pipdt})(\text{dmit})]$ whose whole ESA spectrum is blue-shifted relative to the Pt analogue. This is manifested by a weak maximum at ~ 560 nm, shallow ~ 500 nm bleach and a relatively strong near-UV band with a maximum at ~ 440 nm. SVD analysis (Figure S8-right) shows that the S_1 lifetime of the Ni and Pd complexes is shorter than of their Pt counterparts, 1.44 ps for Ni and ~ 1.9 ps for Pd. The T_1 lifetime of $[\text{Ni}(\text{Pr}_2\text{pipdt})(\text{dmit})]$ is very short, ~ 15 ps, whereas $\gg 500$ ps lifetimes were found for the Pd and Pt complexes. The T_1 state of the Pd complexes undergoes 19-20 ps cooling, slower than in the case of Pt complexes.

Intersystem crossing dynamics

As was explained above (Figure 7), the optically populated S_1 state undergoes parallel intersystem crossing to the lowest triplet state T_1 and nonradiative transition to the ground state (GS). Kinetics of these two processes can be disentangled using the measured singlet-state lifetime values τ_S and quantum yields of the hot triplet population ($QY_{S \rightarrow \#T}$): $\tau_{\text{ISC}} = \tau_S / QY_{S \rightarrow \#T}$ and $\tau_S^{-1} = \tau_{\text{ISC}}^{-1} + \tau_{\text{nR}}^{-1}$. The $QY_{S \rightarrow \#T}$ values (Table 1) were determined as the ratio of the GSB amplitude after the S_1 depopulation to the initial amplitude after the femtosecond solvation-driven relaxation step τ_1 . (For instance, in case of $[\text{Pt}(\text{Pr}_2\text{pipdt})(\text{dmit})]$ in DMF, we calculated $QY_{S \rightarrow \#T}$ from Figure S4 as the ratio of the amplitude of the spectrum “ $\tau_2 + \tau_3 + \tau_4 + \tau_5$ ” to the spectrum “ $\tau_3 + \tau_4 + \tau_5$ ” at 750 nm). In a similar way, we calculate the overall yield of the singlet-to-triplet conversion ($QY_{S \rightarrow T}$), while the yield of $\#T_1$ cooling ($QY_{\#T \rightarrow T}$) was determined by comparing the GSB amplitudes before and after the T_1 relaxation (the τ_{TVR} step). It follows that that the triplet yield increases in the order Ni < Pd < Pt (Table 1), which means that the efficiency of the nonradiative channel to the ground state decreases on going down the triad.

Table 2. Estimated time constants (ps) of the intersystem crossing from the singlet excited state to the triplet state (τ_{ISC}) and internal conversion to the ground state (τ_{nr}).

	[Pt(¹ Pr ₂ pipdt)(dmit)]	[Pt(Bz ₂ pipdt)(dsit)]	[Pd(Bz ₂ pipdt)(dmit)]	[Pd(Bz ₂ pipdt)(dsit)]	[Ni(¹ Pr ₂ pipdt)(dmit)]
τ_{ISC}	6.2±0.4	5.7±0.3	5.7±0.3	5.9±0.3	5.8±0.4
τ_{nr}	7.6	17.5	2.8	2.9	1.9

Estimated τ_{ISC} and τ_{nr} values are reported in Table 2. It follows that the ISC rate is essentially independent of the central metal atom occurring with virtually the same time constant of ~6 ps despite the fact that the spin-orbit coupling constant increases in the order Ni < Pd < Pt. Replacing the S donor atoms by heavier Se has no effect either. ISC in the investigated complexes is one to two orders of magnitude slower than in octahedral complexes with low-lying metal-to-ligand CT excited states (30-150 fs).^{20, 22, 24-28} In this respect, the behaviour of planar dithione-dithiolato complexes support our previous notion that ISC rates in transition metal complexes do not scale with the strength of the spin-orbit interaction²² and that the excited state character and symmetry are more important factors than the heavy-metal participation.²⁹⁻³² In the present case of LL'CT excited states, both the singlet and triplet have the same orbital origin, being derived from a HOMO→LUMO excitation (see Figure S1 for the orbital shapes). Hence, S₁ and T₁ are not related by orbital rotation and, therefore, not coupled by spin-orbit interaction, regardless of the heavy-metal involvement and spin-orbit coupling constant. Direct ISC is then symmetry forbidden and the spin conversion has to occur by second order mechanisms, involving either coupling with higher excited states or spin-vibronic interactions. ISC lifetimes found herein are comparable to or little shorter than those measured for other metal complexes where direct ISC is symmetry forbidden, for example, MLCT states of Cu(I) diimines: ~14 ps³³ and Pt(0) phosphines: ~3 ps,³⁴ intraligand excited states of Re(I) complexes (~30 ps),³⁰ and dσ*pσ states of [Pt₂(pop)₄]⁴⁻ (3-30 ps)³² and its perfluoroborated derivative (1.6 ns).³¹

On the other hand, the rate of the S_1 nonradiative decay to the ground state increases in the order $Pt < Pd < Ni$. This trend can be tentatively attributed to a molecular distortion facilitating the vibronic coupling, since the angle between the two ligands increases in the same order: $\sim 0^\circ$, $\sim 5^\circ$, and $\sim 8^\circ$, respectively.¹¹

Assignment of the excited-state absorption and origin of the femtosecond kinetics component.

Based on the prevalent^{9, 14, 15} HOMO \rightarrow LUMO character of the lowest allowed electronic transition and the predominant LUMO localization on the R_2 pipdt dithione ligand (Figure S1-right), it can be expected³⁵ that absorption spectra of both singlet and triplet LL'CT states will resemble the spectrum of the one-electron reduced state, where the LUMO is singly occupied. Spectroelectrochemical reduction of $[Pt(Bz_2pipdt)(dmit)]$ in DMF indeed shows¹¹ a disappearance of the 760 nm and 480 nm bands and formation of a strong band at 560 nm and a shoulder at 380 nm, closely resembling the short-time ESA absorption pattern that, however, occurs more in the red: a strong band at 630 nm and a shoulder at 430 nm (Figure 8). The T_1 spectrum, albeit weak, is even closer to that of the monoanion, showing a band at about 560 nm, and absorption increasing into the UV. The similarity between the early-time ESA and the absorption spectrum of the monoreduced $[Pt(Bz_2pipdt)(dmit)]^-$ provides a good evidence for the predominant localization of the excited electron at Bz_2pipdt in both S_1 and T_1 . Accordingly, the intensity of the S_1 ESA band at 630 nm is expected to increase with the fractional electron charge on the R_2 pipdt moiety.

This is a good starting point to discuss the femtosecond rise of the ESA intensity and of the negative bleach signal that were found to occur for all investigated complexes with the time constant in the 300-760 fs range (Table 1). Above, it was shown for $[Pt(^iPr_2pipdt)(dmit)]$ that the time constants measured in MeCN (300 fs) and DMF (760 fs) scale with the characteristic solvent relaxation time:²³ 150 and 670 fs, respectively. Hence, we attribute the

femtosecond dynamics to solvation-driven charge redistribution in the excited molecule. In particular, optical excitation by the femtosecond pump pulse occurs in the Franck-Condon regime, without any change in the molecular structure and solvation, but with a large change in the molecular dipole moment (as high as 11 D for the investigated complexes).⁹ However, at the moment of excitation, the solvent dipoles are oriented as in the ground state and exert an electric field ("reaction field") that hinders the excitation-induced charge transfer from dmit/dsit to R₂pipdt. A fast solvent reorientation follows, which optimizes solvation according to the new molecular charge distribution and, via solute-solvent interactions, drives the charge separation in the excited molecule to completion by changing the excited-state wave function. Experimentally, this is manifested by the rise of the ESA bands that originate from transitions localized at the ligand reduced by excitation. It can thus be argued that the LL'CT excited-state character (formally $^1[M(II)(R_{2}pipdt^{\bullet-})(dmit/dsit^{\bullet-})]$) of S₁ is fully developed only after this ultrafast solvent relaxation step. This conclusion is supported by the match between the inverted and scaled first DAS (τ_1) with the DAS corresponding to the S₁ population decay, see Figure S9. Alternatively, one may consider attributing the ultrafast relaxation τ_1 to intramolecular vibrational redistribution (IVR). However, IVR is usually very fast (few tens of femtoseconds), as has been revealed by the "instantaneous" fluorescence Stokes shift observed for various metal diimine complexes^{22, 24, 25, 27, 36} as well as organic dyes.²³

The molecules investigated herein are planar, apparently not undergoing any specific solvation with MeCN or DMF. The solute-solvent interactions that lead both to solvatochromism^{9, 11, 12} and femtosecond solvation dynamics are primarily electrostatic in nature. In this respect, these complexes resemble the coumarin 153 dye that was originally used to determine dynamics of nonspecific solvation dynamics, mostly based on a dielectric solvent response.²³ The common nonspecific/electrostatic nature of solvation explains the match between the solvation dynamics determined with coumarin 153²³ and metal dithione-

dithiolato complexes. An increase of the ESA intensity at short times after excitation also has been observed for $^3\text{MLCT}$ states of rhenium and ruthenium 2,2'-bipyridine (bpy) complexes, occurring, however, on a much slower timescale, up to 20 ps.^{25, 26, 37, 38} In these complexes, the ESA rise concerns mostly the typical³⁵ ~ 380 nm band of $\text{bpy}^{\bullet-}$ and was attributed to a solvation-driven charge separation in the $\text{M} \rightarrow \text{bpy } ^3\text{MLCT}$ state. The much slower lifetime compared with the dithiolene case is likely caused by the 3D structure of pseudooctahedral Re and Ru complexes that allows for solvent clustering around the molecule and solvational relaxation requiring more extensive restructuring of the solvent shell.³⁹

The increase (deepening) of the GSB signal was observed for the dithione-dithiolato complexes only. It is tentatively rationalized by assuming that the Franck-Condon excited state (i.e., before developing the LL'CT charge separation) possesses a weak ground-state like absorption bands whose intensities decrease in the course of solvation-driven charge separation, manifested by deepening of the GSB signal.

Conclusions:

Pt, Pd, and Ni dithione-dithiolato/diselenolato complexes exhibit a common excited-state behaviour upon irradiation into the lowest absorption band: excitation is followed by hundreds-of-femtoseconds solvation-driven relaxation, which drives the dithiolato/diselenolato \rightarrow dithione charge separation, forming a $^1\text{LL}'\text{CT}$ excited-state (S_1), that can be formally described as $^*1[\text{M}(\text{II})(\text{dithione}^{\bullet-})(\text{dithiolate}/\text{diselenolate}^{\bullet-})]$. Its absorption spectrum resembles that of the reduced $[\text{M}(\text{II})(\text{dithione}^{\bullet-})(\text{dithiolate}/\text{diselenolate}^{2-})]^-$ species. The $^1\text{LL}'\text{CT}$ state undergoes simultaneous decay to the ground state and intersystem crossing (ISC) to the $^3\text{LL}'\text{CT}$, that is populated with a $<50\%$ yield, depending on the metal: $\text{Pt} > \text{Pd} > \text{Ni}$. ISC occurs on a ~ 6 ps timescale, independent of the metal, whereas the rate of the nonradiative decay to the ground state decreases on going from Ni (2 ps) to Pd (3 ps) and Pt

(~10 ps). The triplet state is long-lived ($\gg 500$ ps) for Pt and Pd complexes and short lived for Ni (~15 ps). Some of the investigated complexes exhibit spectral changes due to vibrational cooling of the singlet (2-3 ps) as well as the triplet (7-18 ps). Both these relaxation processes are accompanied by partial GS recovery. Rotational diffusion occurs with lifetimes in the 120-200 ps range, sometimes becoming biphasic (40, 190 ps), presumably due to anisotropic rotation of the planar molecule. Changing the dithione ($\text{Bz}_2\text{pipdt}/^i\text{Pr}_2\text{pipdt}$) as well as dithiolate/diselenolate (dmit/dsit) ligands has only very small effects on the photobehavior.

Because of their planarity, apparent lack of specific solvation, large dipole moment change upon excitation, and exceptional hyperpolarizability, dithione-dithiolato complexes are highly sensitive to the local electrostatics. Their $^1\text{LL}'\text{CT}$ excited-state spectra show distinct temporal evolution on the femtosecond timescale, whose rates in DMF and MeCN scale with solvent relaxation rates determined with a coumarin 153 dye.²³ After $^3\text{MLCT}$ states of Re(I) and Ru(II) diimine complexes, $^1\text{LL}'\text{CT}$ excited states of dithione-dithiolate complexes present another example of solvation-driven charge separation that is manifested by increasing intensity of the ESA band due to a transition localized on the photoreduced ligand, establishing this effect as more general: taking place in different excited states and different coordination geometries. It follows, that TA absorption spectra of CT states on a fs-ps timescale can be used as reporters of solvation-related charge localization processes.

The independence of the ISC rate on the metal (Ni, Pd, Pt) and the donor atom (S, Se) underlies the notion²² that the strength of spin-orbit coupling is not the decisive factor determining ISC dynamics in series of structurally related metal complexes. Instead, ISC is governed by factors such as the excited-state character, molecular geometry, symmetry of the molecular orbitals being depopulated and populated in the singlet and triplet excited states, and vibronic couplings. In the present case, both the singlet and triplet LL'CT states are derived from the same one-electron excitations, involving the same MOs. Hence, the two

states are not related by rotation and direct ISC is therefore forbidden. In this respect, $^1,^3\text{LL}'\text{CT}$ states resemble $\pi\pi^*$ intraligand excited states, for which slow ISC has been observed even in complexes of heavy Re or Rh atoms.^{30,40}

Possible photonic applications would likely be based on the presence of the lowest S_1 ($^1\text{MMLCT}$) electronic transition and excited state, since the T_1 transition is forbidden and the T_1 ($^3\text{MMLCT}$) state is populated with a low yield (<50%). Metal dithione-dithiolate complexes are potential candidates for redox switchability of their NLO response.¹¹⁻¹³ Transient NLO also has been considered.⁴¹ Strong and reversible S_1 excited-state absorption observed herein indicates possible uses of these complexes as optical limiters and saturable dyes that were reported⁴²⁻⁴⁴ for homoleptic dithiolene complexes. Of a special interest are possible applications as photosensitizers of light-energy harvesting. Strong visible absorption extending into NIR, photostability, and reversible redox reactivity of metal dithione-dithiolates are promising prerequisites. Estimating the S_1 ($^1\text{LL}'\text{CT}$) energy as 1.4 eV and taking the first reduction potential¹¹⁻¹⁴ as -0.2 V (vs. NHE), we can estimate the S_1 excited-state reduction potential as ca. $+1.2$ V (vs. NHE), indicating that $[\text{M}(\text{R}_2\text{dipdt})(\text{dmit}/\text{dsit})]$ complexes could behave as strong photooxidants. The $1.4 - 4.5$ ps $^1\text{LL}'\text{CT}$ lifetimes are long enough to allow for ultrafast electron transfer, either when attached to p-type semiconductors,⁴⁵ in supramolecular assemblies, or in dinuclear complexes, where a metal dithione-dithiolato sensitizers would be electronically well coupled to a photocatalyst.

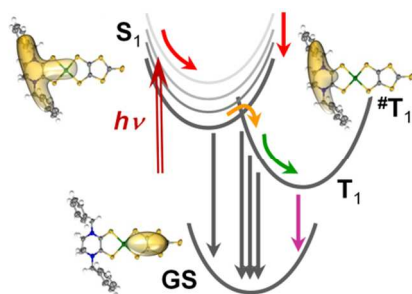
Acknowledgments

This research was carried out in the framework of European collaboration programme COST Action CM1202 PERSPECT-H₂O. Financial support from the ERC Starting Grant 279599-FunctionalDyna), Swiss NSF through the NCCR MUST "Molecular Ultrafast Science and Technology", Fondazione Banco di Sardegna and Università di Cagliari, Ministry of

Education of the Czech Republic (grant LD14129), COST CM1202, is gratefully acknowledged.

1. V. Balzani, P. Ceroni and A. Juris, *Photochemistry and Photophysics*, Wiley-VCH, Weinheim, 2014.
2. R. Eisenberg and H. B. Gray, *Inorg. Chem.*, 2011, 50, 9741–9751.
3. S. Sproules and K. Wieghardt, *Coord. Chem. Rev.*, 2011, 255, 837–860.
4. M. D. Ward and J. A. McCleverty, *J. Chem. Soc., Dalton Trans.*, 2002, 275–288.
5. G. Bruno, M. Almeida, F. Artizzu, J. C. Dias, M. L. Mercuri, L. Pilia, C. Rovira, X. Ribas, A. Serpe and P. Deplano, *Dalton Trans.*, 2010, 39, 4566 – 4574.
6. G. Bruno, M. Almeida, D. Simão, M. L. Mercuri, L. Pilia, A. Serpe and P. Deplano, *Dalton Trans.*, 2009, 495-503.
7. J. A. McCleverty, *Prog. Inorg. Chem.*, 1968, 10, 49-221.
8. K. D. Karlin and E. I. Stiefel, *Dithiolene Chemistry. Synthesis, Properties and Applications.*, J. Wiley & Sons, Hoboken, 2004.
9. P. Deplano, L. Pilia, D. Espa, M. L. Mercuri and A. Serpe, *Coord. Chem. Rev.*, 2010, 254, 1434–1447.
10. S. Curreli, P. Deplano, C. Faulmann, A. Ienco, C. Mealli, M. L. Mercuri, L. Pilia, G. Pintus, A. Serpe and E. F. Trogu, *Inorg. Chem.*, 2004, 43, 5069-5079.
11. D. Espa, L. Pilia, L. Marchiò, M. L. Mercuri, A. Serpe, A. Barsella, A. Fort, S. J. Dalgleish, N. Robertson and P. Deplano, *Inorg. Chem.*, 2011, 50, 2058–2060.
12. L. Pilia, D. Espa, A. Barsella, A. Fort, C. Makedonas, L. Marchiò, M. L. Mercuri, A. Serpe, C. A. Mitsopoulou and P. Deplano, *Inorg. Chem.*, 2011 50, 10015–10027.
13. D. Espa, L. Pilia, L. Marchiò, M. Pizzotti, N. Robertson, F. Tessore, M. L. Mercuri, A. Serpe and P. Deplano, *Dalton Trans.*, 2012, 41, 12106-12113.
14. D. Espa, L. Pilia, L. Marchiò, F. Artizzu, A. Serpe, M. L. Mercuri, D. Simão, M. Almeida, M. Pizzotti, F. Tessore and P. Deplano, *Dalton Trans.*, 2012, 41, 3485-3493.
15. D. Espa, L. Pilia, C. Makedonas, L. Marchiò, M. L. Mercuri, A. Serpe, A. Barsella, A. Fort, C. A. Mitsopoulou and P. Deplano, *Inorg. Chem.*, 2014, 53, 1170–1183.
16. E. A. M. Geary, L. J. Yellowlees, S. Parsons, L. Pilia, A. Serpe, M. L. Mercuri, P. Deplano, S. J. Clark and N. Robertson, *Dalton Trans.*, 2007, 5453-5459.
17. E. A. M. Geary, L. J. Yellowlees, L. A. Jack, I. D. H. Oswald, S. Parsons, N. Hirata, J. R. Durrant and N. Robertson, *Inorg. Chem.*, 2005, 44, 242-250.
18. J. Zhang, P. Du, J. Schneider, P. Jarosz and R. Eisenberg, *J. Am. Chem. Soc.*, 2007, 129, 7726-7727.
19. W. Paw, S. D. Cummings, M. A. Mansour, W. B. Connick, D. K. Geiger and R. Eisenberg, *Coord. Chem. Rev.*, 1998, 171, 125-150.
20. W. Gawelda, A. Cannizzo, V.-T. Pham, F. van Mourik, C. Bressler and M. Chergui, *J. Am. Chem. Soc.*, 2007, 129, 8199-8206.
21. J. Helbing, L. Bonacina, R. Pietri, J. Bredenbeck, P. Hamm, F. van Mourik, F. Chaussard, A. Gonzalez-Gonzalez, M. Chergui, C. Ramos-Alvarez, C. Ruiz and J. Lopez-Garriga, *Biophysical Journal*, 2004, 87.
22. A. Cannizzo, A. M. Blanco-Rodríguez, A. Nahhas, J. Šebera, S. Zális, A. Vlček, Jr. and M. Chergui, *J. Am. Chem. Soc.*, 2008, 130, 8967-8974.
23. M. L. Horng, J. A. Gardecki, A. Papazyan and M. Maroncelli, *J. Phys. Chem.*, 1995, 99, 17311-17337.

24. A. Cannizzo, F. van Mourik, W. Gawelda, G. Zgrablic, C. Bressler and M. Chergui, *Angew. Chem. Int. Ed.*, 2006, 45, 3174-3176.
25. A. El Nahhas, C. Consani, A. M. Blanco-Rodríguez, K. M. Lancaster, O. Braem, A. Cannizzo, M. Towrie, I. P. Clark, S. Záliš, M. Chergui and A. Vlček, Jr., *Inorg. Chem.*, 2011, 50, 2932–2943.
26. A. El Nahhas, A. Cannizzo, F. van Mourik, A. M. Blanco-Rodríguez, S. Záliš, A. Vlček, Jr. and M. Chergui, *J. Phys. Chem. A*, 2010, 114, 6361-6369.
27. O. Bräm, F. Messina, E. Baranoff, A. Cannizzo, M. K. Nazeeruddin and M. Chergui, *J. Phys. Chem. C* 2013, 117, 15958–15966.
28. O. Bräm, A. Cannizzo and M. Chergui, *Phys. Chem. Chem. Phys.*, 2012, 14, 7934–7937.
29. M. Chergui, *Dalton Trans.*, 2012, 41, 13022-13029
30. A. M. Blanco-Rodríguez, H. Kvapilová, J. Sýkora, M. Towrie, C. Nervi, G. Volpi, S. Záliš and A. Vlček, Jr., *J. Am. Chem. Soc.*, 2014, 136, 5963–5973.
31. A. C. Durrell, G. E. Keller, Y.-C. Lam, J. Sýkora, A. Vlček, Jr. and H. B. Gray, *J. Am. Chem. Soc.*, 2012, 134, 14201–14207.
32. R. M. van der Veen, A. Cannizzo, F. van Mourik, A. Vlček, Jr. and M. Chergui, *J. Am. Chem. Soc.*, 2011, 133, 305-315.
33. Z. A. Siddique, Y. Yamamoto, T. Ohno and K. Nozaki, *Inorg. Chem.*, 2003, 42, 6366-6378.
34. Z. A. Siddique, T. Ohno and K. Nozaki, *Inorg. Chem.*, 2004, 43, 663-673.
35. S. Záliš, C. Consani, A. El Nahhas, A. Cannizzo, M. Chergui, F. Hartl and A. Vlček, Jr., *Inorg. Chim. Acta*, 2011, 374, 578–585.
36. O. Bräm, F. Messina, A. M. El-Zohry, A. Cannizzo and M. Chergui, *Chem. Phys.*, 2012, 393, 51–57.
37. D. J. Liard, M. Busby, P. Matousek, M. Towrie and A. Vlček, Jr., *J. Phys. Chem. A*, 2004, 108, 2363-2369.
38. S. Wallin, J. Davidsson, J. Modin and L. Hammarström, *J. Phys. Chem. A*, 2005, 109, 4697-4704.
39. M.-E. Morel, I. Tavernelli and U. Rothlisberger, *J. Phys. Chem. B* 2009, 113, 7737–7744.
40. A. Steffen, M. G. Tay, A. S. Batsanov, J. A. K. Howard, A. Beeby, K. Q. Vuong, X.-Z. Sun, M. W. George and T. B. Marder, *Angew. Chem. Int. Ed.*, 2010, 49, 2349 – 2353.
41. P. Aloukos, S. Couris, J. B. Koutselas, G. C. Anyfantis and G. C. Papavassiliou, *Chem. Phys. Lett.*, 2006, 109–113.
42. K. T. Müller-Westerhoff, in *Comprehensive Coordination Chemistry*, ed. G. Wilkinson, Pergamon, Oxford, 1987, p. 595.
43. D. Qing, C. X. Feng, C. Hong, G. Xing, Z. X. Ping and C. Zhusheng, *Supramol. Sci.*, 1998, 5, 531-536.
44. K. H. Drexhage and K. T. Müller-Westerhoff, *IEEE J. Quantum Electron.*, 1972, QE-8, 759.
45. F. Odobel, Y. Pellegrin, E. A. Gibson, A. Hagfeldt, A. L. Smeigh and L. Hammarström, *Coord. Chem. Rev.*, 2012, 256, 2414– 2423.



LL'CT excited states of Pt, Pd, Ni dithione-dithiolates undergo subpicosecond solvation-driven charge redistribution and ≈ 6 ps metal-independent intersystem crossing.